Kobe University Repository : Kernel

PDF issue: 2025-12-05

X-ray photoelectron spectroscopy-based valence band spectra of passive films on titanium

Eda, Yuzuki ; Manaka, Tomoyo ; Hanawa, Takao ; Chen, Peng ; Ashida, Maki ; Noda, Kazuhiko

(Citation)
Surface and Interface Analysis,54(8):892-898

(Issue Date)
2022-08

(Resource Type)
journal article

(Version)
Version of Record

(Rights)
© 2022 The Authors. Surface and Interface Analysis published by John Wiley & Sons Ltd. This is an open access article under the terms of the Creative Commons Attribution-NonCommercial-NoDerivs License, which permits use and distribution in any medium, provided the original work is properly cited, the use is non-commercial and no…

(URL)
https://hdl.handle.net/20.500.14094/90009508

Check for updates

Received: 24 November 2021 | Revised: 7 March 2022 | Accepted: 12 April 2022

DOI: 10.1002/sia.7102

RESEARCH ARTICLE

SURFACE and INTERFACE ANALYSIS WILEY

X-ray photoelectron spectroscopy-based valence band spectra of passive films on titanium

Yuzuki Eda[1] | Tomoyo Manaka[2] | Takao Hanawa[3,4] | Peng Chen[3] | Maki Ashida[3] | Kazuhiko Noda[1]

[1]Department of Materials Science and Engineering, Shibaura Institute of Technology, Tokyo, Japan

[2]Department of Metallic Biomaterials, Graduate School of Medical and Dental Sciences, Tokyo Medical and Dental University, Tokyo, Japan

[3]Department of Metallic Biomaterials, Institute of Biomaterials and Bioengineering, Tokyo Medical and Dental University, Tokyo, Japan

[4]Center for Advanced Medical Engineering Research & Development, Kobe University, Kobe, Japan

Correspondence
Takao Hanawa, Department of Metallic Biomaterials, Institute of Biomaterials and Bioengineering, Tokyo Medical and Dental University, 2-3-10 Kanda-surugadai, Chiyoda-ku, Tokyo 101-0062, Japan.
Email: hanawa.met@tmd.ac.jp

Funding information
Ministry of Education, Culture, Sports, Science and Technology (MEXT), Japan; Biable Materials Project; Design & Engineering by Joint Inverse Innovation for Materials Architecture Project

[Correction added on 13 June 2022, after first online publication: The copyright line was changed.]

Titanium (Ti) is always covered by thin passive films. Thus, valence band (VB) spectra, obtained using X-ray photoelectron spectroscopy (XPS), are superpositions of the VB spectra of passive films and that of the metallic Ti substrate. In this study, to obtain the VB spectra only of passive films, angular resolution (for eliminating the substrate Ti contribution) and argon ion sputtering (for removing passive films) were used along with XPS. The passive film on Ti was determined to consist of a very thin TiO_2layer with small amounts of Ti_2O_3, TiO, hydroxyl groups, and water with a thickness of 5.9 nm. The VB spectra of Ti were deconvoluted into four peak components: a peak at ~1 eV, attributed to the Ti metal substrate; a broad peak in the 3–10 eV range, mainly attributed to O 2p (~6 eV) and O 2p-Ti 3d hybridized states (~8 eV), owing to the π (non-bonding) and σ (bonding) orbitals in the passive oxide film; and a peak at ~13 eV, attributed to the 3σ orbital of O 2p as OH^-or H_2O. The VB region spectrum between approximately 3 and 14 eV from Ti is originating from the passive film on Ti. In particular, characterization of VB spectrum obtained with a takeoff angle of less than 24° is effective to obtain VB spectrum only from the passive film on Ti. The property as *n*-type semiconductor of the passive film on Ti is probably higher than that of rutile TiO_2ceramics.

KEYWORDS
passive film, titanium, valence band, X-ray photoelectron spectroscopy

1 | INTRODUCTION

Titanium (Ti) is always covered by surface oxide in the form of passive films, which contributes to the excellent corrosion resistance of Ti. A typical passive film covering a Ti consists mainly of a very thin amorphous TiO_2 layer with small amounts of Ti_2O_3, TiO, water, and hydroxyl groups.[1–4] In addition, the composition is graded: More Ti^{4+} and OH^- are found near the film's surface.[3] This oxidation process of the formation of the passive film has been discussed in a previous study.[5] The chemical state of the passive film has been precisely characterized, and its local fine structure has been clarified.[6] The composition, structure, and chemical state of the passive film were reported to differ from those of crystalline TiO_2 ceramics; the surface properties of the passive film were reported to differ from those of

This is an open access article under the terms of the Creative Commons Attribution-NonCommercial-NoDerivs License, which permits use and distribution in any medium, provided the original work is properly cited, the use is non-commercial and no modifications or adaptations are made.
© 2022 The Authors. *Surface and Interface Analysis* published by John Wiley & Sons Ltd.

TiO_2 ceramics.[7] Most of the above studies were conducted for core-level electron binding energy region spectra obtained using X-ray photoelectron spectroscopy (XPS).

On the other hand, as is well known, the reactivity of TiO_2 ceramics is governed by the band gap, E_g, between the valence band (VB) and the conduction band (CB), and the effort to decrease E_g continues.[8] The E_g value of the photocatalyst decreases as its optical response shifts toward longer excitation wavelengths. There are several methods for minimizing the photocatalyst E_g. The basic strategy is to create impurity/defect states in the bulk to enable low-energy photoexcitation. From this viewpoint, a passive film on Ti naturally contains oxygen defects because the composition is non-stoichiometric, as mentioned earlier. Therefore, differences between the surface properties of passive films on Ti and bulk TiO_2 ceramics may be owing to the difference between their E_g values. The E_g value for a passive film on Ti after anodic and thermal oxidation was determined using the photo-electrochemical technique,[9–11] because conventional techniques for oxide ceramics (such as ultraviolet absorption) cannot be applied to thin oxide films.

In any case, the VB structure near the Fermi energy level, E_F, is important for understanding the reactivity of passive films on Ti. However, as mentioned previously, Ti is always covered by thin passive films, so the XPS spectrum in the VB range is a superposition of the spectrum attributed to the passive film and that of the substrate metallic Ti. A lot of studies on VB structure of TiO_2 ceramics are performed both by theoretical calculation and experimental characterization, whereas there is no study on that of the passive films on metal substrate by theoretical calculation because the composition and chemical state are complicated. The composition and chemical states are graded to depth direction, and hydroxyl groups and water are contained. The passive films on Ti are different from defect-containing simple oxides such as TiO_2 ceramics. Therefore, to characterize VB structure of the passive film on Ti, XPS characterization was attempted in this study. To obtain the VB spectra only for passive films, angular resolution was used for eliminating the Ti substrate contribution. In addition, for comparison, a spectrum only owing to the Ti substrate was obtained after argon ion-based sputtering for removing the passive film. These spectra were then compared with those of TiO_2 ceramics to obtain the VB spectrum only attributed to the passive film on Ti. The precise investigation of the VB XPS spectra is likely to improve our understanding of the electron structure of the passive film on Ti.

2 | EXPERIMENTAL PROCEDURE

2.1 | Preparation of commercially pure Ti and TiO_2 specimens

A commercially pure Ti (99.5%; Grade 2; Test Materials, Tokyo, Japan) rod (diameter, 8 mm) was cut into disks (thickness, 1.5 mm). The disks were mechanically polished and cleaned ultrasonically, as described previously.[4] In addition, polycrystalline rutile TiO_2 disks were prepared by sintering the TiO_2 powder compact. The details have been described elsewhere.[7]

2.2 | XPS

XPS was performed using an electron spectrometer (JPS-9010MC, JEOL, Tokyo, Japan). All binding energies reported in the present work are relative to E_F, and all of the spectra were excited using the Mg Kα line (1253.6 eV). Pass energy was 50 and 20 eV for wide scan and narrow scan, respectively. Under this condition, the full width at half maximum (FWHM) of a peak originating from Ag $3d_{5/2}$ electron was 0.9 eV. The spectrometer was calibrated against Au $4f_{7/2}$ (binding energy, 84.07 eV) and Au $4f_{5/2}$ (binding energy, 87.74 eV) of pure Au, as well as Cu $2p_{3/2}$ (kinetic energy, 932.53 eV), Cu $2p_{1/2}$ (kinetic energy, 952.35 eV), and the Cu Auger $L_3M_{4,5}M_{4,5}$ line (kinetic energy, 918.65 eV) of pure Cu. These energy values were based on published data.[12] The binding energies were calibrated with respect to a peak (285.0 eV) owing to an apparent contaminant in the C 1s electron energy region. To estimate the photoelectron peak intensities, backgrounds were subtracted from the measured spectra using Shirley's method.[13] The composition and thickness of the surface oxide film were simultaneously calculated as previously reported[14,15] and explained elsewhere.[4,16,17] The angle-resolved technique for XPS was applied to Ti at the photoelectron takeoff angles of 12°, 24°, 37°, 53°, and 90°, corresponding to the detection depths of 0.2λ, 0.4λ, 0.6λ, 0.8λ, and 1.0λ, where λ was the photoelectrons' effective mean free path. The effective escape depth was estimated as λ times the sine of the takeoff angle. The takeoff angle was defined as the angle between the direction of the photoelectron path to the electron spectrometer and the specimen surface. Argon ion sputtering was performed under appropriate conditions (500 V and mA cm^{-2} in 8×10^{-2} Pa for 1800 s) for removing the passive film. This argon ion sputtering condition was determined after several trials. In the case of the argon ion sputtering, the binding energies were calibrated with respect to a peak (454.0 eV) in the Ti 2p electron energy region, owing to metallic Ti, because C 1s region peak from surface contamination was unclear. For argon-ion-sputtered Ti and rutile TiO_2, the detection angle was 90° (1.0λ). In addition, polycrystalline rutile TiO_2 ceramics were characterized for comparison.

3 | RESULTS

3.1 | Core-level spectra using the angle-resolved technique

Carbon, nitrogen, oxygen, and Ti were detected in all of the analyzed specimens. The spectra of the Ti 2p electron energy regions obtained from Ti detected at 90° from the specimens' surfaces are shown in Figure 1A. The peaks were deconvoluted to reveal the component peaks attributed to the different chemical states. The Ti 2p spectrum exhibited four doublets, according to valence: the metallic state of Ti^0 and the oxide states of Ti^{2+}, Ti^{3+}, and Ti^{4+}. Published data[2] were used

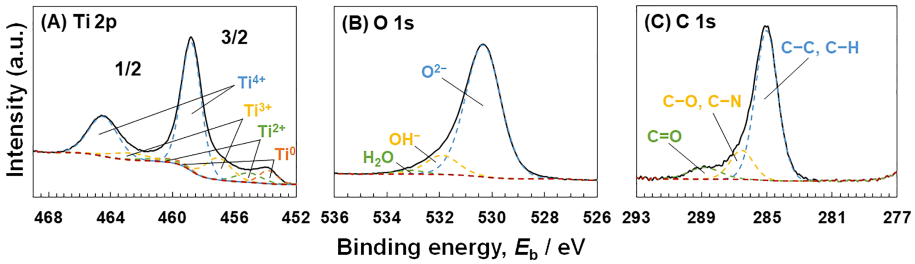

FIGURE 1 Ti 2p (A), O 1s (B), and C 1s (c) electron energy region spectra of Ti, for the takeoff angle of 90°, and their deconvolutions into component peaks

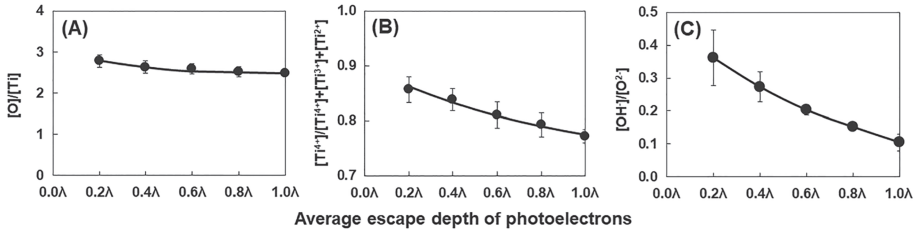

FIGURE 2 The ratios of [O]/[Ti] (A), $[Ti^{4+}]/([Ti^{4+}] + [Ti^{3+}] + [Ti^{2+}])$ (B), and $[OH^-]/[O^{2-}]$ (C), plotted against the average escape depth of photoelectrons ($n = 3$)

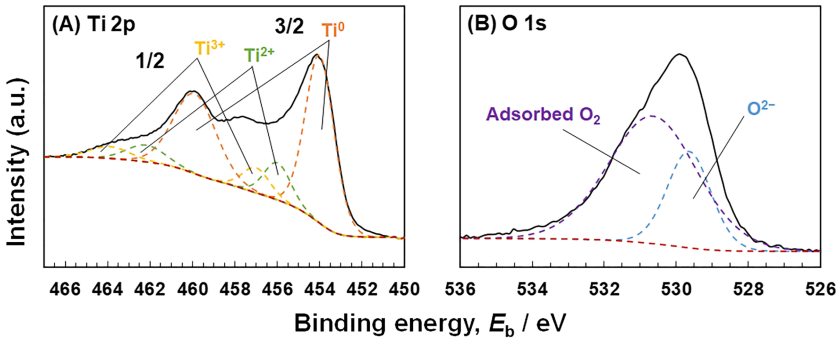

FIGURE 3 Ti 2p (A) and O 1s (B) electron energy region spectra of Ti, after argon sputtering, and their deconvolutions into component peaks

for determining the binding energies of the different Ti valence states. The proportions of $[Ti^0]$, $[Ti^{2+}]$, $[Ti^{3+}]$, and $[Ti^{4+}]$ obtained for the takeoff angle of 90° (1.0λ) were 0.06, 0.07, 0.15, and 0.72, respectively (mean values, $n = 3$); the proportions of $[Ti^{2+}]$, $[Ti^{3+}]$, and $[Ti^{4+}]$ were 0.07, 0.16, and 0.77, respectively (mean values, $n = 3$). As shown in Figure 1B, the O 1s region spectrum contained three peaks originating from O^{2-}, hydroxide or hydroxyl groups, OH^-, and hydrate or adsorbed water, H_2O.[18] The proportions of $[O^{2-}]$, $[OH^-]$, and $[H_2O]$ obtained for 90° were 0.86, 0.09, and 0.05, respectively (mean values, $n = 3$). The relative concentrations of Ti and oxygen obtained for 90° were 28.8 ± 1.1 at.% and 71.2 ± 1.1 at.% ($n = 3$), respectively. The calculated thickness of the passive film was 5.9 ± 0.1 nm ($n = 3$), similar to a previously reported value.[4] Therefore, the passive film on Ti consisted of a very thin TiO_2 layer with small amounts of Ti_2O_3, TiO, hydroxyl groups, and water, consistent with previous reports.[1–4] As shown in Figure 1C, the C 1s region spectrum in all specimens was deconvoluted into three peaks, originating from C–C and C–H (285.0 eV), C–O and C–N (~287 eV), and C–O (~289 eV) as so-called contamination layer.[19] The thickness of the contamination layer was calculated as 0.4–0.7 nm that was almost one-tenth that of the passive film (5.9 nm). Therefore, the influence of contamination layer on VB region spectra is small.

Regarding the average effective escape depth of photoelectrons as assessed by angle-resolved XPS measurements, λ was the average mean free path of Ti 2p and O 1s photoelectrons, and the effective escape depth was estimated as λ times the sine of the takeoff angle. Figure 2A shows the ratio of the relative concentration of oxygen to that of Ti, [O]/[Ti], against the average escape depth of the photoelectrons. Oxygen was more abundant in the outer layer, whereas Ti was more abundant in the inner layer of the passive film. The proportion of the integrated intensity of the peak attributed to Ti^{4+} relative to all of the oxide states of Ti, $[Ti^{4+}]/([Ti^{4+}] + [Ti^{3+}] + [Ti^{2+}])$, obtained using the angle-resolved technique, is shown in Figure 2B. At small takeoff angles, the proportion of Ti^{4+} was high, suggesting that Ti^{4+} was distributed more in the outer layer than in the inner layer of the passive film. In addition, the depth profiles of the $[OH^-]/[O^{2-}]$ ratios are shown in Figure 2c, revealing that OH^- was more abundant in the outer layer of the passive film.

3.2 | Core-level spectra obtained using argon ion sputtering

After several trials, it was recognized that it is impossible to remove oxygen completely by argon ion sputtering, because sputtered oxygen atoms were immediately adsorbed and started to form oxides owing to the high chemical activity of Ti atoms, even in a high-vacuum environment. Figure 3 shows the Ti 2p and O 1s electron energy region

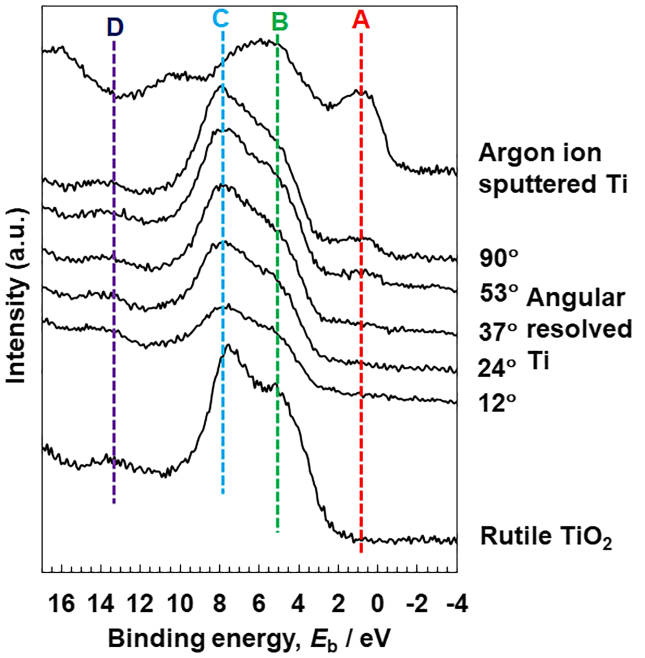

FIGURE 4 VB region spectra of Ti, for the takeoff angles of 90°, 53°, 37°, 24°, and 12°, argon ion sputtered Ti, and rutile TiO_2

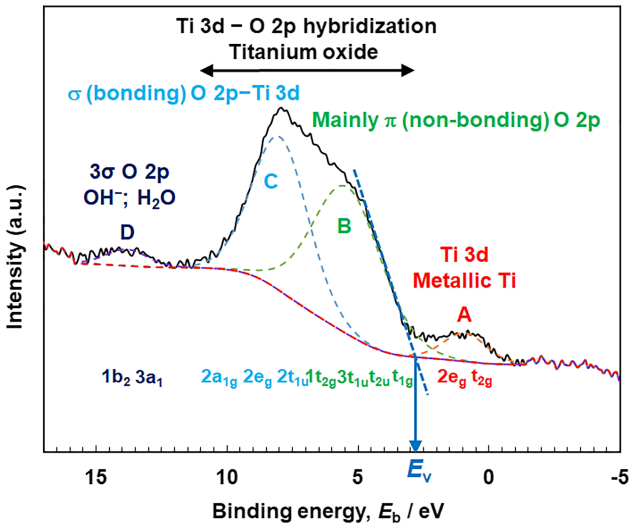

FIGURE 5 VB region spectra of Ti, for the detection angle of 90°, with its deconvolution into component peaks, originating orbits, and the determination of the maximal energy of the VB, E_v

spectra of Ti, obtained following argon ion sputtering. The Ti 2p region spectrum exhibited three doublets, according to valence: the metallic state of Ti^0 and the oxide states of Ti^{2+} and Ti^{3+}. The proportions of [Ti^0], [Ti^{2+}], and [Ti^{3+}] were 0.72, 0.18, and 0.10, respectively (mean values, $n = 3$), and the proportions of [Ti^{2+}] and [Ti^{3+}] were 0.65 and 0.35, respectively (mean values, $n = 3$). On the other hand, the O 1s electron energy region spectrum was deconvoluted into two peaks. The peak at approximately 530 eV originated from O^{2-} combined with Ti^{2+} and Ti^{3+}. The other peak at approximately 531 eV is usually originated from OH^-. However, it is hard to exist as OH^- for oxygen after argon ion sputtering, although binding energy of O 1s electron form adsorbed oxygen, O_2, is approximately 531 eV.[20] Assuming that only the integrated intensity of the peak at approximately 530 eV contributed to the passive oxide film, the relative concentration of oxygen was 54.4 at.%, in a good agreement with the concentration of 54.3 at.% that was calculated based on the concentration of Ti and proportions of Ti^{2+} and Ti^{3+}. Therefore, the peak at approximately 531 eV was not attributed to hydroxide or hydroxyl groups, but to adsorbed O_2. Then, the O 1s region peak was deconvoluted into two peaks, attributed to O^{2-} and adsorbed O_2. The thickness of the oxide layer was 0.6 nm after argon ion sputtering.

3.3 | VB region spectra

Typical VB region spectra of Ti for the angular-resolved technique and for argon ion sputtering are shown in Figure 4. This figure also shows the VB region spectrum of polycrystalline rutile TiO_2. The major peak at VB energy region is located between 3 and 10 eV relative to E_F. This peak is sometimes deconvoluted into three[21–23] and five[24–26] component peaks without physical meaning attached to the modelled components, although the VB spectrum consists of two distinct maxima separated in binding energy by approximately 2.5 eV based on physical orbitals in most of previous studies.[27–33] Therefore, the major peak between 3- and 10-eV peak was deconvoluted into two peaks. In other words, VB region spectra were deconvoluted into four peak components: Peak A at approximately 1 eV, continuous beyond 0 eV (E_F), broad Peak B at approximately 5 eV, Peak C at approximately 8 eV, and Peak D in the 11–14 eV window. Component Peaks B and C were detected in all of the analyzed specimens. Component Peak A was detected for the takeoff angles of 90° and 53°, but not for the takeoff angles of 35°, 24°, and 12°. Peak A was also absent in rutile TiO_2. The integrated intensity of Peak A was the highest for 90°. In addition, the integrated intensity of Peak A was significantly higher after argon ion sputtering.

4 | DISCUSSION

Using the angular-resolved technique, as shown in Figure 2, the relative concentration of oxygen was found to be higher at the surface of the passive film, compared with the bulk region. At the surface, the fraction of Ti^{4+} was higher than those of Ti^{3+} and Ti^{2+}. More OH^- was present at the surface. For the takeoff angles of 24° and 12°, metallic Ti substrate was not detected (Figure 4), indicating that the only contribution to the VB spectrum at these angles was from the passive film.

Chemical state of the oxide layer is changed by argon ion sputtering, because the sputtering efficiency of oxygen is much larger than that of titanium. As a result, the preferential sputtering of oxygen atom, thereby decreasing the oxygen to titanium ratio, and the surface

oxide will be reduced and more Ti^{3+} and Ti^{2+} appeared. Thus, spectra obtained from the argon-ion-sputtered surface is not an original spectrum of a deeper surface region. During argon ion sputtering, sputtered oxygen immediately readsorbed by titanium to regenerate oxide because of high chemical activity of titanium atom. The spectra shown in this study are obtained at a certain moment during the above ongoing process. Therefore, the adsorbed O_2 was detected. Sputtering and regeneration of oxide are repeated during argon ion sputtering, and complete removal of oxide from titanium substrate is impossible, although the thickness of the oxide is decreased by argon ion sputtering with change in the chemical state. However, the purpose of argon ion sputtering is reducing the influence of surface oxide from a resultant VB spectrum, in other words, the strengthening the influence of metal Ti substrate on the resultant VB spectrum. We attempted to decrease the thickness of the passive film on Ti substrate as possible. In this regard, the thickness was actually decreased. Therefore, this purpose is achieved by argon ion sputtering in this study. Therefore, after argon ion sputtering, the passive film contributed less to the VB spectrum, compared with the substrate metallic Ti.

The VB region spectra were deconvoluted into Peaks A, B, C, and D, as shown in Figure 5. VB spectra have been investigated in many studies from the viewpoint of the photocatalysis of TiO_2 ceramics. In nanocrystalline and amorphous TiO_2, VB spectra exhibited resonance enhancement for binding energies in the 2–10 eV range, populated by the O 2p and hybridized Ti 3d states.[34] In the case of anatase, the VB spectrum exhibited two peaks, a rather broad one at approximately 6 eV, and a narrower one at approximately 8 eV; these corresponded mainly to π (non-bonding) and σ (bonding) O 2p orbitals, respectively.[27,28] The same result was reported for rutile.[29] The Ti 3d contribution to the 8-eV peak must be higher than that to the 5.7-eV peak, because the 8.0-eV peak resonated stronger than the 5.7-eV peak. The VB spectrum in the 3–10 eV range mostly reflected the presence of O 2p (approximately 5.5 eV) and O 2p-Ti 3d hybridized states (approximately 7.5 eV) in the oxide layer, but the Ti 3d partial density of states spreads all VB.[21–23,30,35] The oxygen VB is composed of a variety of orbitals: t_{1g}, t_{2u}, $3t_{1u}$, $1t_{2g}$, $2t_{1u}$, $2e_g$, and $2a_{1g}$. Among these, the $1t_{2g}$ and $2e_g$ orbitals are π and σ bonding to the Ti 3d states, with 12% and 21% charge density at each Ti site, respectively. The hybridization between Ti and O 2p states extends over the whole VB, and the Ti 3d contribution dominates in the lower two-thirds of the VB.[36,37] On the other hand, the VB is mainly of O 2p origin (80%), but it also contains 13% Ti 3d and 7% of the other symmetries.[33] Therefore, Peaks B and C were attributed to the π (non-bonding) and σ (bonding) O 2p orbitals, respectively, hybridized with Ti 3d states. The above discussion is reflected to orbitals shown in Figure 5.

The presence of a peak at approximately 1 eV below E_F is in general attributed to sub-stoichiometric Ti^{3+} ions.[11] Ti^{3+} defect states are located in the band gap at 0.7–0.9 eV below E_F, and the peak at approximately 1.3 eV has already been attributed to oxygen vacancies at the surface, which give rise to Ti^{3+} species.[27,38] Owing to defect-induced Ti 3d states just below E_F, argon-ion bombardment of TiO_2 (110) reduced the emission intensity from O 2p non-bonding orbitals,[22] although the 0–3 eV region corresponds to the metallic Ti 3d character of the sub-stoichiometric oxides at the interface and the metallic Ti substrate below.[21] On the other hand, a peak originating from adsorbed hydroxyl groups locates at approximately 1.4 eV.[25,34,38–40] A peak located at 0.8 eV is also observed to rise monotonically with increasing H_2O exposure.[40] However, in this study, this peak was not present for 35°, 24°, and 12°, though it became more prominent following argon ion sputtering. Therefore, Peak A detected in this study was mainly attributed to the Ti metal substrate; the influence of the Ti^{3+} defect or H_2O exposure on peak A was small. Relatively large peak at 0–3 eV is observed from Ti.[24] In addition, peaks originated from metallic Ti locate at 0.5, 1.25, and 1.6 eV.[41] The Ti VB is composed of 3d orbitals: t_{2g} and e_g. Therefore, Peak A was straddled from the VB to E_F in the CB, because it originated from the metallic state.

The 3σ orbital of OH^- was responsible for the VB spectral feature at the binding energy of approximately 10.8 eV, and organic contaminants could introduce an extra feature at approximately 11 eV.[31] The $1b_2$ molecular orbital of H_2O is aligned with the peak at 13.2 eV and the $1b_2$ feature of molecular water and the 3σ orbital of dissociated water to lie at around 13 and 11 eV, respectively.[39] The binding energy of the 3σ state of OH^- is close to that of the $3a_1$ state of molecular water. The 3σ OH^- feature at 11.4 eV is higher in intensity than the $1b_2$ state of the molecular water located at 13.2 eV, suggesting the presence of hydroxyls. Peak D was detected in all angular-resolved specimens as well as rutile TiO_2, but was not detected for argon-ion-sputtered Ti. Therefore, Peak D originated from the 3σ orbital of O 2p as OH^- or H_2O.

VB region spectrum between approximately 3 and 14 eV from Ti, Peaks B, C, and D in Figures 4 and 5, is originating only from the passive film on Ti, whereas peak at 0–3 eV, Peak A, is not originating from the passive film but from metallic Ti substrate. In particular, characterization of VB spectrum obtained with a takeoff angle of less than 24° is effective to obtain VB spectrum only from the passive film on Ti.

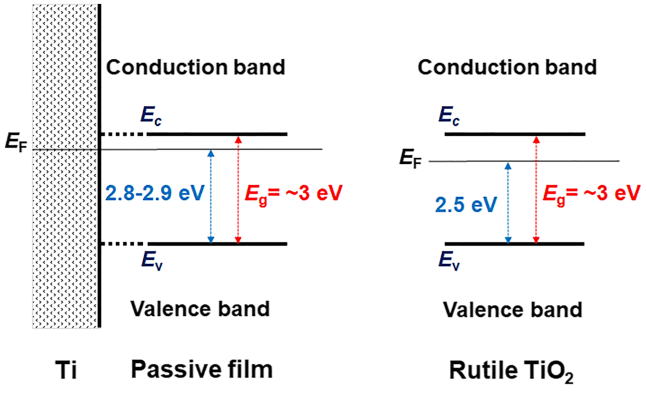

FIGURE 6 Difference in E_v against E_F between band structures of the passive film on Ti and rutile TiO_2 ceramics

The maximal energy of the VB, E_v, was determined by linearly extrapolating the peak to the baseline,[34] as shown in Figure 5. The value of E_v was almost constant, at 2.8–2.9 eV, for the different takeoff angles; this value was higher than that for rutile, which was at 2.5 eV. The E_v value for the as-deposited TiO_2 film was observed at 1.86 eV.[34] Therefore, the E_v value for the passive film on Ti was higher than that for TiO_2 ceramics. Difference in E_v against E_F between the passive film on Ti and rutile TiO_2, as shown in Figure 6. In other words, the energy between minimum energy of CB, E_c, and E_F of the passive film on Ti is smaller than that of rutile TiO_2. Therefore, the property as *n*-type semiconductor of the passive film on Ti is probably higher than that of rutile TiO_2 ceramics if their E_gs are identical as approximately 3 eV.

5 | CONCLUSIONS

The passive film on Ti was determined to consist of a very thin TiO_2 layer with small amounts of Ti_2O_3, TiO, hydroxyl groups, and water, and its thickness was 5.9 nm. Oxygen, Ti^{4+}, and OH^- were more abundant in the outer layer than in the inner layer of the passive film. It was impossible to remove oxygen completely by argon ion sputtering, but residual O^{2-} combined with Ti^{2+} and Ti^{3+} and adsorbed O_2 were detected after argon ion sputtering. The VB spectra were deconvoluted into four peak components: a peak at approximately 1 eV continuing beyond 0 eV (E_F), a broad peak at approximately 6 eV, a peak at approximately 8 eV, and a peak at approximately 13 eV. The peak at approximately 1 eV, detected in this study, was attributed to the Ti metal substrate. The peaks in the 3–10 eV region corresponded mainly to the O 2p (at approximately 6 eV) and O 2p-Ti 3d hybridized states (at approximately 8 eV) and were attributed to the π (non-bonding) and σ (bonding) orbitals in the passive oxide film. The peak at approximately 11–14 eV was attributed to the 3σ orbital of O 2p as OH^- or H_2O. Therefore, the peak in the 3–14 eV range, detected from Ti, was attributed to the passive film on Ti. More π (non-bonding) O 2p orbitals existed at the surface of the passive film. The VB region spectrum between approximately 3 and 14 eV from Ti is originating only from the passive film on Ti. In particular, characterization of VB spectrum obtained with a takeoff angle of less than 24° is effective to obtain VB spectrum only from the passive film on Ti. The property as *n*-type semiconductor of the passive film on Ti is probably higher than that of rutile TiO_2 ceramics if their E_gs are identical. The findings of the present study can be used for characterizing reactions of Ti with surrounding environments, such as biological tissues.

ACKNOWLEDGMENTS

This work was supported by the Design & Engineering by Joint Inverse Innovation for Materials Architecture Project, Biable Materials Project, and Research Center for Biomedical Engineering, Ministry of Education, Culture, Sports, Science and Technology (MEXT), Japan.

ORCID

Yuzuki Eda https://orcid.org/0000-0002-8476-7369
Tomoyo Manaka https://orcid.org/0000-0001-9649-2035
Takao Hanawa https://orcid.org/0000-0003-1688-1749
Peng Chen https://orcid.org/0000-0002-5131-6043
Maki Ashida https://orcid.org/0000-0003-0007-0407
Kazuhiko Noda https://orcid.org/0000-0003-0582-9654

REFERENCES

1. Kelly EJ. Electrochemical behavior of titanium. *Mod Aspects Electrochem*. 1982;14:319-424. doi:10.1007/978-1-4615-7458-3_5
2. Asami K, Chen SC, Habazaki H, Hashimoto K. The surface characterization of titanium and titanium-nickel alloys in sulfuric acid. *Corros Sci*. 1993;35(1–4):43-49. doi:10.1016/0010-938X(93)90131-Y
3. Hanawa T, Asami K, Asaoka K. Repassivation of titanium and surface oxide film regenerated in simulated bioliquid. *J Biomed Mater Res*. 1998;40(4):530-538. doi:10.1002/(SICI)1097-4636(19980615)40:4<530::AID-JBM3>3.0.CO;2-G
4. Hiji A, Hanawa T, Shimabukuro M, Chen P, Ashida M, Ishikawa K. Initial formation kinetics of calcium phosphate on titanium in Hanks solution characterized using XPS. *Surf Interface Anal*. 2021;53(2):185-193. doi:10.1002/sia.6900
5. Olver JW, Ross JW Jr. On the standard potential of the titanium (III)-titanium (II) couple. *J Am Chem Soc*. 1963;85(17):2565-2566. doi:10.1021/ja00900a006
6. Wang L, Yu H, Wang K, Xu H, Wang S, Sun D. Local fine structural insight into mechanism of electrochemical passivation of titanium. *Appl Mater Interface*. 2016;8(28):18608-18619. doi:10.1021/acsami.6b05080
7. Hiji A, Hanawa T, Yokoi T, Chen P, Ashida M, Kawashita M. Time transient of calcium and phosphate ion adsorption by rutile crystal facets in Hanks solution characterized by XPS. *Langmuir*. 2021;37(12):3597-3604. doi:10.1021/acs.langmuir.0c03540
8. Diebold U. The surface science of titanium dioxide. *Surf Sci Rep*. 2003;48(5–8):53-229. doi:10.1016/S0167-5729(02)00100-0
9. Di Quarto F, Piazza S, Sunseri C. The photoelectrochemistry of thin passive layers. Investigation of anodic oxide films on titanium metal. *Electrochim Acta*. 1993;38(1):29-35. doi:10.1016/0013-4686(93)80006-L
10. Marsh J, Gorse D. A photoelectrochemical and ac impedance study of anodic titanium oxide films. *Electrochim Acta*. 1998;43(7):659-670. doi:10.1016/S0013-4686(97)00210-7
11. Kim DY, Kwon H. A study on electronic properties of passive film formed on Ti. *Corros Sci Technol*. 2003;2:212-218.
12. Asami K. A precisely consistent energy calibration method for X-ray photoelectron spectroscopy. *J Electron Spectrosc*. 1976;9(5):469-478. doi:10.1016/0368-2048(76)80065-5
13. Shirley DA. High-resolution x-ray photoemission spectrum of the valence bands of gold. *Phys Rev B*. 1972;5(12):4709-4714. doi:10.1103/PhysRevB.5.4709
14. Asami K, Hashimoto K, Shimodaira S. XPS determination of compositions of alloy surfaces and surface oxides on mechanically polished iron-chromium alloys. *Corros Sci*. 1977;17(9):713-723. doi:10.1016/0010-938X(77)90067-1
15. Asami K, Hashimoto K. An XPS study of the surfaces on Fe-Cr, Fe-Co and Fe-Ni alloys after mechanical polishing. *Corros Sci*. 1984;24(2):83-97. doi:10.1016/0010-938X(84)90039-8
16. Hanawa T, Ota M. Calcium phosphate naturally formed on titanium in electrolyte solution. *Biomaterials*. 1991;12(8):767-774. doi:10.1016/0142-9612(91)90028-9
17. Tanaka Y, Nakai M, Akahori T, et al. Characterization of air-formed surface oxide film on Ti-29Nb-13Ta-4.6Zr alloy surface using XPS

and AES. *Corros Sci*. 2008;50(8):2111-2116. doi:10.1016/j.corsci.2008.06.002
18. Asami K, Hashimoto K. The X-ray photo-electron spectra ofseveral oxides of iron and chromium. *Corros Sci*. 1977;17(7):559-570. doi:10.1016/S0010-938X(77)80002-4
19. Hammond JS, Holubka JW, de Vries JE, Dickie RA. The application of X-ray photo-electron spectroscopy: a study of interfacial composition-induced paint de-adhesion. *Corros Sci*. 1981;21(3):239-253. doi:10.1016/0010-938X(81)90033-0
20. Ruzankin S, Zilberberg I, Zhidomirov GM. Closed and open-sgell atomic oxygen on silver: two distinct patterns of O1s binding energy and X-ray absorption O K-edge spectra as revealed by density functional theory. *Res Chem Intermed*. 2004;30(1):75-85. doi:10.1163/156856704322798061
21. Breeson AC, Sankar G, Goh GKL, Palgrave RG. Phase quantification by X-ray photoemission valence band analysis applied to mixed phase TiO_2 powders. *Appl Surf Sci*. 2017;423:205-209. doi:10.1016/j.apsusc.2017.06.161
22. Zhang Z, Jeng SP, Henrich VE. Cation-ligand hybridization for stoichiometric and reduced TiO_2 (110) surfaces determined by resonant photoemission. *Phys Rev B*. 1991;43(14):12004-12011. doi:10.1103/PhysRevB.43.12004
23. Thomas AG, Flavell WR, Kumarasinghe AR, et al. Resonant photoemission of anatase TiO_2(101) and (001) single crystals. *Phys Rev B*. 2003;67(3):035110. doi:10.1103/PhysRevB.67.035110
24. Krishna DNG, George RP, Philip J. Determination of nanoscale titanium oxide thin film phase composition using X-ray photoelectron spectroscopy valence band analysis. *Thin Solid Films*. 2019;681:58-68. doi:10.1016/j.tsf.2019.04.044
25. Krishna DNG, Anushree C, George RP, Philip J. Phase identification in binary mixture of nanopowders from deconvoluted valence band spectra using X-ray photoelectron spectroscopy: Case study with iron oxide and titania polymorphs. *Appl Surf Sci*. 2018;462:932-943. doi:10.1016/j.apsusc.2018.08.132
26. Hardman PJ, Raikar GN, Muryn CA, et al. Valence-band structure of TiO_2 along the G-D-X and G-S-M directions. *Phys Rev B*. 1994;49(11):7170-7177. doi:10.1103/PhysRevB.49.7170
27. Caruso T, Lenardi C, Agostino RG, et al. Electronic structure of cluster assembled nanostructured TiO_2 by resonant photoemission at the Ti $L_{2,3}$ edge. *J Chem Phys*. 2008;128(9):094704. doi:10.1063/1.2832321
28. Sanjinés R, Tang T, Berger H, Gozzo F, Margaritondo G, Lévy F. Electronic structure of anatase TiO_2 oxide. *J Appl Phys*. 1994;75(6):2945-2951. doi:10.1063/1.356190
29. Orendorz A, Wüsten J, Ziegler C, Gnaser H. Photoelectron spectroscopy of nanocrystalline anatase TiO_2 films. *Appl Surf Sci*. 2005;252(1):85-88. doi:10.1016/j.apsusc.2005.02.002
30. Sánchez-Agudo M, Soriano L, Trigo JF, et al. Factor analysis applied to the study of valence band resonant photoemission spectra in transition-metal compounds. *Surf Interface Anal*. 2002;34(1):244-247. doi:10.1002/sia.1292
31. Fusi M, Maccallini E, Caruso T, et al. Surface electronic and structural properties of nanostructured titanium oxide grown by pulsed laser deposition. *Surf Sci*. 2011;605(3–4):333-340. doi:10.1016/j.susc.2010.10.039
32. Tezuka Y, Shin S, Agui A, Fujisawa M, Ishii T, Yagishita A. Resonant soft X-ray fluorescence study of rutile (TiO_2). *J Electron Spectrosc*. 1996;79:195-198. doi:10.1016/0368-2048(96)02835-6
33. Pollini I, Mosser A, Parlebas JC. Electronic, spectroscopic and elastic properties of early transition metal compounds. *Phys Rep*. 2001;355(1):1-72. doi:10.1016/S0370-1573(01)00018-7
34. Singh AP, Kodan N, Mehta BR. Enhancing the photoelectrochemical properties of titanium dioxide by thermal treatment in oxygen deficient environment. *Appl Surf Sci*. 2016;372:63-69. doi:10.1016/j.apsusc.2016.03.072
35. Prince KC, Dhanak VR, Finetti P, et al. 2p resonant photoemission study of TiO_2. *Phys Rev B*. 1997;55(15):9520-9523. doi:10.1103/PhysRevB.55.9520
36. Fischer DW. X-ray band spectra and molecular-orbital structure of rutile TiO_2. *Phys Rev B*. 1972;5(11):4219-4226. doi:10.1103/PhysRevB.5.4219
37. Göpel W, Anderson JA, Frankel D, et al. Surface defects of TiO_2(110): A combinated XPS, XAES and ELS study. *Surf Sci*. 1984;139(2–3):333-346. doi:10.1016/0039-6028(84)90054-2
38. Kurtz RL, Stock-Bauer R, Msdey TE, Román E, de Segovia JL. Synchrotron radiation studies of H_2O adsorption on TiO_2(110). *Surf Sci*. 1989;218(1):178-200. doi:10.1016/0039-6028(89)90626-2
39. Di Valentin C, Tilocca A, Selloni A, et al. Adsorption of water on reconstructed rutile TiO_2(011)-(2X1): Ti=O double bonds and surface reactivity. *J Am Chem Soc*. 2005;127(27):9895-9903. doi:10.1021/ja0511624
40. di Valentin C, Pacchioni G, Selloni A. Electronic structure of defect states in hydroxylated and reduced rutile TiO_2(110) surfaces. *Phys Rev Lett*. 2006;97(16):166803. doi:10.1103/PhysRevLett.97.166803
41. Eastman DE. Ultraviolet photoelectron spectroscopy studies of noble and transition metals. In: Shirley DA, ed. *Electron Spectroscopy*. North-Holland Publishing; 1972:487-514.

SUPPORTING INFORMATION

Additional supporting information may be found in the online version of the article at the publisher's website.

How to cite this article: Eda Y, Manaka T, Hanawa T, Chen P, Ashida M, Noda K. X-ray photoelectron spectroscopy-based valence band spectra of passive films on titanium. *Surf Interface Anal*. 2022;54(8):892-898. doi:10.1002/sia.7102